Observation of localized surface plasmons in spatially controlled array structures

2009 Nanotechnology 20 305202

(http://iopscience.iop.org/0957-4484/20/30/305202)

Nanotechnology **20** (2009) 305202 (6pp) doi:10.1088/0957-4484/20/30/305202

Observation of localized surface plasmons in spatially controlled array structures

J W Chou[1], Kao-Chin Lin[1], Yao-Jen Lee[2], Chi-Tsu Yuan[3], Fu-Kuo Hsueh[2], Hsun-Chuan Shih[1], Wen-Chung Fan[1], Chih-Wei Luo[1], Ming-Chieh Lin[4], Wu-Ching Chou[1] and Der-San Chuu[1,5]

[1] Department of Electrophysics, National Chiao Tung University, Hsinchu 30050, Taiwan
[2] National Nano Device Laboratories, Hsinchu 30078, Taiwan
[3] Research Center for Applied Sciences, Academia Sinica, Taipei 11529, Taiwan
[4] Department of Physics, Fu Jen Catholic University, Taipei County 24205, Taiwan

E-mail: dschuu@mail.nctu.edu.tw

Received 28 February 2009, in final form 27 May 2009
Published 7 July 2009
Online at stacks.iop.org/Nano/20/305202

Abstract
We observed the reflectance spectra of three different nano-scale array structures of Au-coated silicon nanorods. The trends of the reflectance spectra indicate that the localized surface plasmon modes can be spatially controlled by manipulating geometric parameters, namely the lattice constants of the array. In addition, the experimental results were compared with 2D numerical simulations based on the finite element method. Satisfactory agreement between the experimental observations and numerical results was obtained.

1. Introduction

Surface plasmons (SP) are waves that propagate along the interface of a metal and dielectric [1, 2] material. A combined excitation consisting of a surface plasmon and a photon is called a surface plasmon polariton (SPP) [3–7]. In addition to SP on a plane surface, excitations of electron plasmons bounded in geometries such as bumps or voids are called localized surface plasmons (LSP). Because of the relatively higher loss and in-plane radiation of the SPP modes, the LSP modes dominate enhancement effects. To distinguish the SPP and LSP modes, one can compare the field enhancement effects at locations near metal surfaces with those far away from metallic surfaces [8]. The field enhancement effects at distances far from a metal surface due to SPP modes tend to be much weaker than those caused by LSP modes. By properly arranging the geometric configuration of a metal/dielectric interface the properties of the SP modes, in particular their interaction with light, can be manipulated. Therefore, many possible applications such as surface enhanced Raman scattering (SERS) [9–12], plasmon waveguides [13], filters, and nanocavities [14] have been developed and improved in recent years. Experimental results from many different particle configurations vary widely in terms of the reported enhancement or quenching. In this paper we designed three different array structures, i.e. square periodic arrays of Au-coated silicon nanorods (SiNRs), to investigate the localized surface plasmons (LSP). The results show that the LSP modes can be manipulated. To study more of the modulated LSP modes, the finite element method (FEM) [15] which is commonly used for solving partial differential equations over complex domains is a good choice. Based on electromagnetic theory, 2D FEM simulations were carried out to obtain the near field optical properties, especially the field distribution of the array structures.

2. Experiment

In our experiments periodic SiNR arrays on Si(100) wafers (n-type, 27 Ω cm) were fabricated by electron beam lithography (EBL) followed by TCP etching. After the SiNR arrays were constructed, 50 nm thick gold thin films were deposited on the surfaces by an electron gun. Three samples of Au-coated SiNRs of the same diameter but with different shortest root distances (210, 380, and 650 nm) between the nearest neighbor Au-coated SiNR arrays were prepared for measurements of the reflectance spectra. Every single Au coated SiNR (in the

[5] Author to whom any correspondence should be addressed.

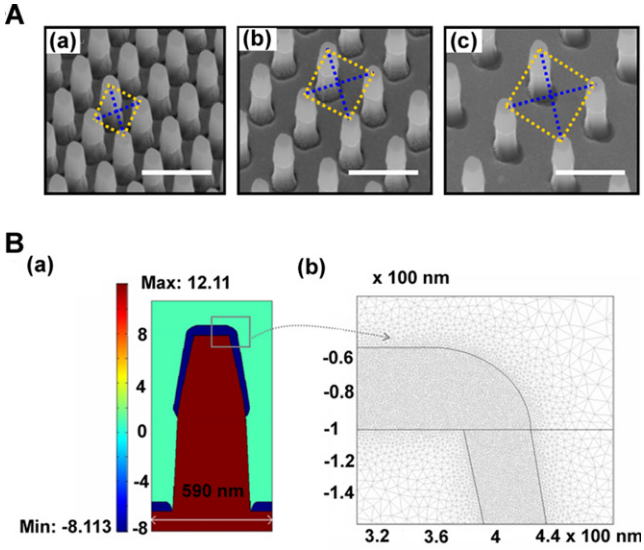

Figure 1. A: SEM images of Au-coated SiNR arrays (a)–(c). Scale bars shown in (a)–(c) are 1 μm. In the square unit cell of each array both the peripheral distances ($D \sim 210$, 380, and 650 nm (yellow dashed line)) and the diagonal distances ($\sqrt{2}D \sim 297$, 537, 919 nm (blue dashed line)) between the two Au-coated SiNRs were included in 2D FE calculations. In (B) (a), a unit cell of array (a) is shown. The color code is the real value of the relative permittivity. ($\varepsilon_{\mathrm{Au}} \sim -8.1$, $\varepsilon_{\mathrm{Si}} \sim 12.1$, $\varepsilon_{\mathrm{Air}} \sim 1.0$) for incident wavelength: 600 nm [16]. (B) (b) The mesh diagram.

three array structures) is not uniformly cylindrical. On the top side, the SiNR is coated with Au (the diameter is ∼200 nm), whereas on the root side, SiNR is not coated with Au (the diameter is ∼380 nm), and the length of the SiNR is ∼900 nm. SEM images of the three array structures (Si substrate tilted at an angle of 30°) are shown in figures 1(A)(a)–(c). In figure 1(B)(a), a unit cell of a 2D single Au-coated SiNR of array (a) is shown. The color code is the real value of the relative permittivity ($\varepsilon_{\mathrm{Au}} \sim -8.1$, $\varepsilon_{\mathrm{Si}} \sim 12.1$, $\varepsilon_{\mathrm{Air}} \sim 1.0$) for incident wavelength equal to 600 nm [16].

A standard reflection setup was used in the experiment. Unpolarized white light from a tungsten halogen lamp was focused on the sample. The spot size is smaller than the size of the sample but much bigger than the lattice constants of the arrays. Thus, inside the region of the spot size (0.2 cm × 0.7 cm) the light can illuminate every Au-coated SiNR uniformly. In reflectance spectra measurements, an incident angle of 5° from the normal direction was set for the three different array structures. The reflection spectra from three arrays of Au-coated SiNRs on Si substrates were normalized to that of 50 nm Au thin films without array structures on the same Si substrates.

3. Results

The reflectance spectra of three different array structures were observed and the results are shown in figures 2(a)–(d). Reflectance spectra labeled 'array (a)', 'array (b)' and 'array (c)' shown in figures 2(a)–(d) correspond to the array structures shown in the SEM images of figures 1(A)(a)–(c), respectively. As shown in figure 2(a), the original reflectance spectra with the LSP resonances in each sample are within the wavelength region ranging from 550 to 850 nm. The LSP modes of the three arrays are labeled by arrows 'sp_n' as shown in figures 2(a)–(d), where: sp_1, $\mathrm{sp}_{1'}$ in figure 2(b) are the group for the highest frequencies; sp_2 in figure 2(c) are

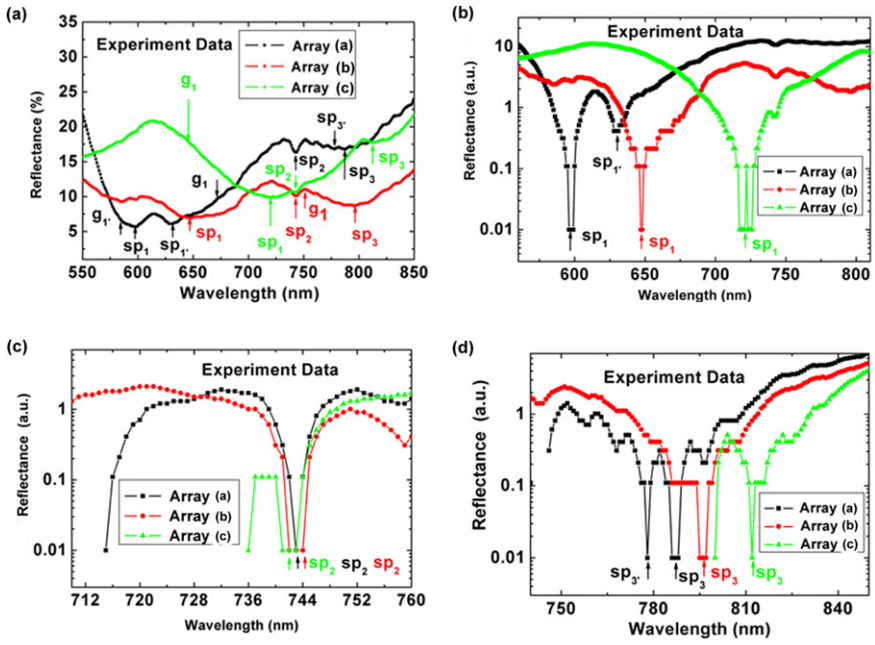

Figure 2. Reflectance spectra of three arrays. In (a) the original reflectance spectra of arrays (a)–(c) within the wavelength region 550–850 nm are shown. The LSP modes (labeled by arrows 'sp_n') and the grating effects (labeled by arrows 'g_1', '$\mathrm{g}_{1'}$') of arrays (a)–(c) are shown. (b)–(d) The common logarithm of the reflectance curves. In (b) and (d), the highest and the lowest frequencies of the LSP modes are shown in the spectra. In (c), the resonances of the LSPs at $\lambda_0 \sim 743$ nm for arrays (a)–(c) (labeled by arrows 'sp_2') are displayed; they show the unique feature of a single Au-coated SiNR.

Table 1. Table listing the peripheral distances and the diagonal distances (D, $\sqrt{2}D$), the incident wavelengths of the LSP modes (sp_1, $sp_{1'}$, sp_2, sp_3, $sp_{3'}$) of arrays (a)–(c) observed in the reflectance spectra; 2D FEM simulations results—the incident wavelengths at the extra sharp peak values of the time average total energy enhancement factor curves for the grating effects (g_1, $g_{1'}$) and the peak (or dip) values of the enhancement factor curves for the LSP modes (sp_1, $sp_{1'}$, sp_2, sp_3, $sp_{3'}$) of arrays (a)–(c).

Array	D, $\sqrt{2}D$ (nm)	Spectra: sp_1, $sp_{1'}$: λ_0 (nm)	FEM: sp_1, $sp_{1'}$: λ_0 (nm)	Spectra: sp_2: λ_0 (nm)	FEM: sp_2: λ_0 (nm)	Spectra: $sp_{3'}$, sp_3: λ_0 (nm)	FEM: $sp_{3'}$, sp_3: λ_0 (nm)	FEM: $g_{1'}$, g_1: λ_{ij} (nm)
(a)	210, 297	597, 630	591, 624	743	743	778, 787	781, 786	584, 672
(b)	380, 537	650	660	743	743	797	791	751
(c)	650, 919	721	727	743	743	812	812	646

the group for the other special feature, i.e. the notch is at an incident wavelength of 743 nm; and sp_3, $sp_{3'}$ in figure 2(d) are the group for the lowest frequencies. In order to compare the LSP modes of the three arrays more easily, we shifted the reflectance curves in figures 2(b)–(d) until their dips 'sp_n' value reach 0.01%, and then took the common logarithms of the three reflectance curves, respectively. As shown in figures 2(b)–(d), the longer the distances between Au-coated SiNRs, the lower the frequencies of the LSP modes (red shift), as shown in the reflectance spectra of figures 2(b) and (d).

With a standard setup we can only get information about which incident wavelength the LSP will resonate at. For estimating the SP resonance frequencies, starting from Maxwell's equations under appropriate boundary conditions, one can obtain the SP dispersion relation for the metal–dielectric interface:

$$k_{SP} = k_0\sqrt{\frac{\varepsilon_m\varepsilon_d}{\varepsilon_m + \varepsilon_d}}. \quad (1)$$

Here k_{SP} is the frequency-dependent SP wavevector, ε_m is the frequency-dependent permittivity of the metal and ε_d is the frequency-dependent permittivity of the dielectric material. The SP wavevector (k_{SP}) for a gold–air interface in our spectrum range (550–850 nm) is $1.02k_0$–$1.07k_0$ [16, 17]. According to equation (1), the incident light with a lower frequency produces a higher frequency of LSP mode. This is because $k_{sp} = 1.02k_0$–$1.07k_0$, $k_{sp} > k_0$, therefore, $\nu_{sp} > \nu_0$ ($k = \frac{2\pi\nu}{c}$, where ν is the frequency of light). The relative permittivity of the gold is assumed to follow the Drude model [17] and is frequency dependent. The experimental data of Johnson and Christie [16] were used in our 2D FEM simulations.

For a square array with the lattice constant a_0 and incident wavelengths, λ_{ij} can be recognized approximately from the equation derived from the dispersion relation as shown in equation (1):

$$\lambda_{ij} = \lambda_{max}\sqrt{i^2 + j^2} \cong a_0\sqrt{\frac{\varepsilon_m\varepsilon_d}{\varepsilon_m + \varepsilon_d}}, \quad (2)$$

where indices i and j are the scattering orders from the array [6]. The red shift of the grating effects and the LSP modes of array (a)–(c) can be qualitatively explained by equation (2): when a_0 is tuned to be longer, the LSP modes λ_{ij} are shifted to be longer. However, due to the geometric complexities of our array structures, it is difficult to predict quantitatively the red shifts of LSP modes and the grating effects by simply using equations (1) and (2). We shall employ the 2D FEM to estimate our observed results. In table 1, we list the peripheral and diagonal distances of arrays (a)–(c) used in the simulations, the incident wavelengths of the LSP modes (sp_1, $sp_{1'}$, sp_2, sp_3, $sp_{3'}$) observed in the reflectance spectra, the extra sharp peak (g_1, $g_{1'}$), peak (or dip) (sp_1, $sp_{1'}$, sp_2, sp_3, $sp_{3'}$) values of the time average total energy enhancement factor curves (calculated by 2D FEM as shown in figures 4(a)–(c)). The characteristics of the grating effects are shown in the last column of table 1. (The extra sharp peaks 'g_n' at λ_{ij} calculated from the 2D FEM are listed; $\lambda_{10} = 584$ nm and $\lambda_{10} = 672$ nm are for the peripheral and diagonal directions of array (a), respectively, $\lambda_{10} = 751$ nm is for the peripheral direction of array (b), and $\lambda_{21} = 646$ nm is for the diagonal direction of array (c) inside our wavelength region of interest, 560–850 nm.) λ_{10} for the diagonal direction of array (c) is about 1300 nm which is clear for understanding the red shift characteristic of the grating effect. However, it is outside our wavelength region of interest and is not listed here. Inside our wavelength region of interest only $\lambda_{21} = 646$ nm for array (c) is shown.

4. Discussion

To analyze the reflectance spectra of our specific array structures, we used the FEM simulations as implemented in the FEMLEB code (www.femlab.de) to calculate the time average total energy densities and the enhancement factors of arrays (a)–(c) at every specific incident wavelength. The results are shown in figures 3(A) and (B) and 4(a)–(c). In the simulations, the Helmholtz wave equations were solved within a unit cell by employing periodic boundary conditions for each case. In the square unit cell of each array, both the peripheral distances ($D = 210$, 380, and 650 nm (as shown in figures 1(A)(a)–(c) yellow dashed line)) and the diagonal distances ($\sqrt{2}D \sim 297$, 537, and 919 nm (as shown in figures 1(A)(a)–(c) blue dashed line)) between the two Au-coated SiNRs were included. The convergence of our simulation models has been checked by varying mesh sizes to evaluate the normalized electric field at the center of a Au-coated SiNR with a distance of ~5 nm from the top of the rod. We reduced the mesh size until it was sufficiently fine so that the results do not depend on meshes, avoiding numerical errors [18]. Finally, we chose tiny meshes with a maximum grid size of 2 nm at all Au coating surfaces, and relatively coarse meshes of maximum value 50 nm within the SiNRs, as shown in figure 1(B)(b).

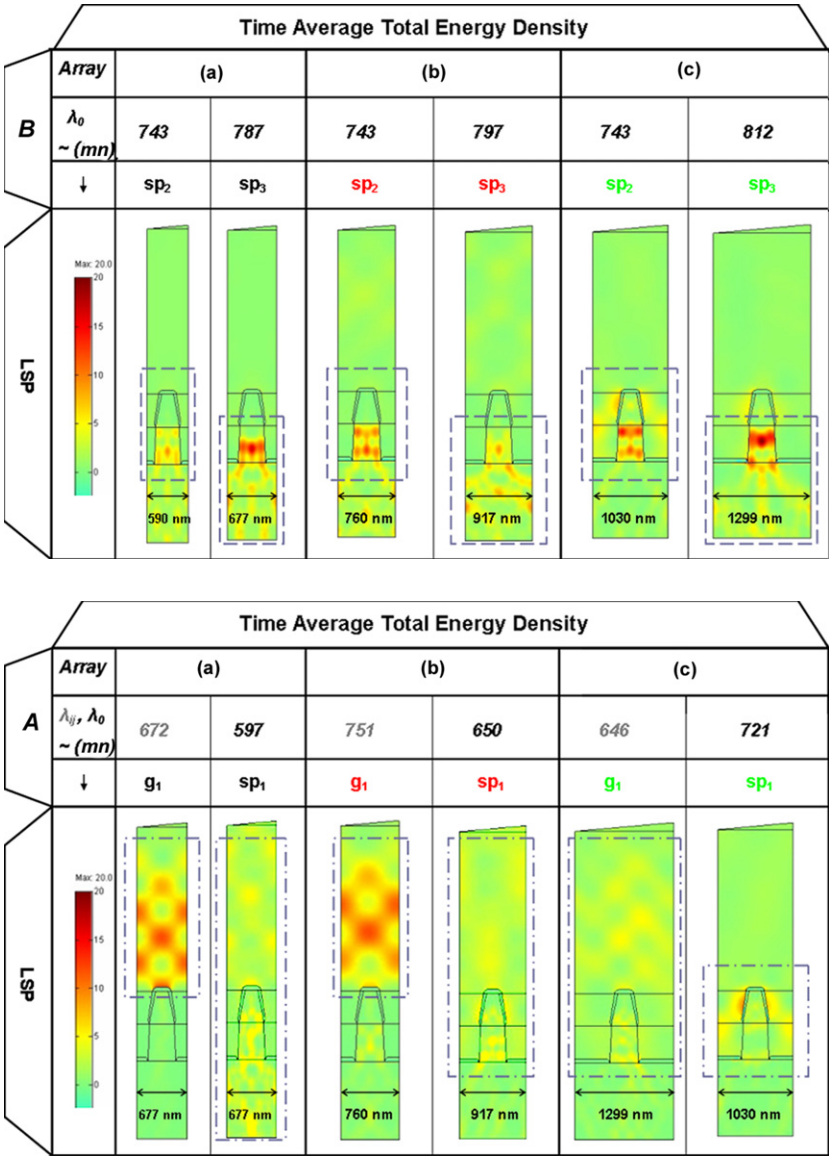

Figure 3. 2D FEM calculations of the normalized time average total energy densities of the three array structures which represent typical examples of LSP modes with the grating effects. The left columns of (A) (a)–(c) show the most obvious grating effects with strong constructive interference happening in the air at different λ_{ij} (labeled by arrow 'g_1') for arrays (a)–(c). The right columns of (A) (a)–(c) present the LSP modes with constructive interference being stronger in the air (labeled 'sp_1'); while the right columns of (B) (a)–(c) present the LSP modes with constructive interference being stronger in the Si (labeled 'sp_3'). The left columns of (B) (a)–(c) show the LSP modes at $\lambda_0 \sim 743$ nm for arrays (a)–(c) (labeled by arrow 'sp_2') to be a unique feature from every single Au-coated SiNR with constructive interference formed inside. The color codes for (A) and (B) are the absolute values of the time average total energy densities normalized to the incident total energy densities.

Figures 3(A)(a)–(c) show the LSP modes accompanied by the constructive interference occurring strongly in the air and slightly in the Si for arrays (a)–(c). Figures 3(B)(a)–(c) show the LSP modes accompanied by the constructive interference occurring strongly in the Si and slightly in the air for arrays (a)–(c). The theoretical counterparts of the typical LSP modes of the three array structures shown in the reflectance spectra (figures 2(a)–(d)) can be found in figures 3(A) and (B) and 4(a)–(c) (marked with 'sp_n'). Among these examples, the LSP modes indicate that the single Au-coated SiNR exhibits its unique feature, i.e. the total energy densities are concentrated inside SiNRs and formed constructive interference inside SiNRs, as shown in figures 3(B)(a)–(c) (the left columns).

A quantitative interpretation of the reflectance spectra requires further investigations. However, some points for qualitative discussion of the reflectance spectra can be given. First of all, the trends of the reflectance spectra can be modulated by varying the lattice constants of Au-coated SiNR arrays. Second, the trends of reflectance spectra are dominated by the LSP modes and the grating effects. We have discussed the first point in detail for figures 2(a)–(d). For second point, the following discussions are given. The valleys shown in the reflectance spectra correspond to the high optical fields produced by the LSP modes and the conditions which are proper for the constructive interference formed inside the Si, whereas the peaks shown in the reflectance spectra correspond

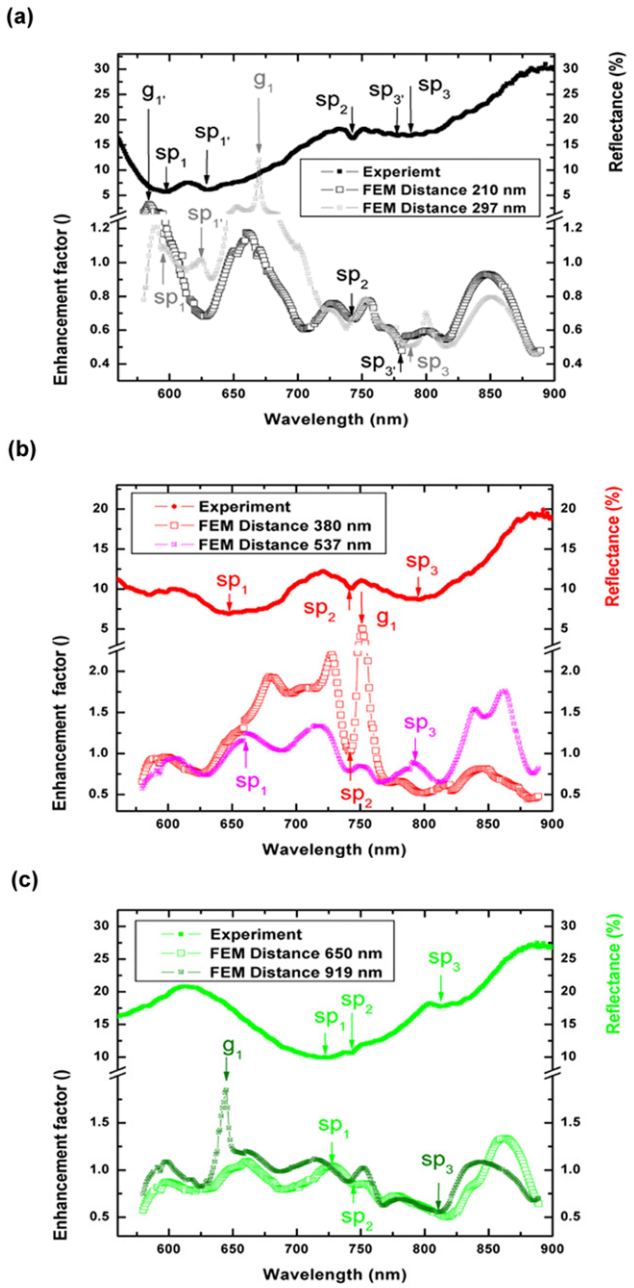

Figure 4. Reflectance spectra of arrays (a)–(c) with 2D FEM simulations of the normalized time average total energy enhancement factors. In each unit cell, both the peripheral and diagonal Au-coated SiNRs are included for calculations. The LSP resonance modes (shown as peaks or dips, labeled by arrows sp_n) and the grating effects (shown as the extra sharp peaks, labeled by arrows g_1, $g_{1'}$) found in 2D FEM simulation results correspond to reflectance spectra.

(This figure is in colour only in the electronic version)

to the grating effects which form constructive interference in the air. Because the optical fields are highly confined at the surface of a metal the propagation of SPs is subject to the significant energy losses. When the frequencies of the incident light are properly matched with those of the LSP resonance modes, the damping effects in the nonconductors are obvious and the corresponding absorption coefficients are increased to reach maximum values. Therefore, low reflection can be observed. In our Au-coated SiNR array structures, the LSPs resonate at the surface of the Au in the nonconductors, i.e. air and Si can both cause low reflectance. As mentioned before, in addition to the LSP modes, the grating effects with constructive interference formed in the nonconductors, i.e. air and Si, can also contribute to the reflectance spectra. The complexity of the analysis increases when the LSP modes are accompanied by grating effects which may cause high reflectance (with constructive interference formed in the air) or low reflectance (with constructive interference formed in the Si).

By 2D FEM, we find that the distributions of the time average total energy densities are strongly dependent on the geometries of the metallic nano-particles and their orientations with respect to the incident fields. Apparently, the LSP modes observed in reflectance spectra as shown in figures 2(a)–(d) manifest the characteristics that the total energy densities are highly concentrated near the surface of a metal, as shown in figures 3(A) and (B). We also obtain the normalized time average total energy enhancement factors in our spectral range by integrating the time average total energy in the area of the top region above the SiNR (height $\sim 2\ \mu$m in the air) of each unit cell for our three array structures with respect to 50 nm Au thin film without any array structures on the Si substrate (the results are show in figures 4(a)–(c) and table 1). One finds that the sharpest peak values of the enhancement factors correspond to the obvious grating effects, as shown in figures 3(A)(a)–(c) (the left column), and the LSP modes appear as the peaks (or dips) in the enhancement factor curves as shown in figures 4(a)–(c). The LSP modes appear as the peaks in the enhancement factor curves when the LSP modes accompanied with the constructive interference formed strongly in air, as shown in figures 3(A)(a)–(c), and appear as the dips when accompanied with constructive interference formed strongly in Si, as shown in figures 3(B)(a)–(c). For all simulations, the incident TM mode plane wave is inclined by 5° to the normal direction of the Si substrate. The color codes in figures 3(A) and (B) indicate the absolute value of the time average total energy density which is normalized by the incident total energy density.

The reason why the sharp peaks 'g_n' obtained by the simulations are missing in the observed spectra can be explained as follows. The simulation result of each array is full angle integration, 0°–180°, which obtained from linear superposition of the TM mode plane wave in the near field regions. This can reveal subtle characteristic of the intensity distributions including the grating effects from higher order diffraction and also more LSP modes. However, in the experimental observations, far field reflection measurements of a 5° reflection angle were performed and one could receive only the zero order diffraction. This is the case in the grating equation: $a_0(\sin\theta_m - \sin\theta_i) = m\lambda$, where a_0 is the lattice constant, θ_m is the diffraction angle, and θ_i is the incident angle. In this case, $\theta_m = \theta_i = 5°$, so that $m = 0$ and the zero order diffraction light is the reflection light itself. At reflection angles of 5° in the far field regions, the higher order diffraction cannot contribute to the rise of the intensity. Therefore, at the

reflection angle, the grating effects (sharp peaks 'g_n') were not observed in reflectance spectra. Owing to this arrangement in experiments which could avoid disturbance of the sharp diffraction peak, the LSP peaks could be clearly extracted from the reflection spectra.

5. Conclusion

Based on electromagnetic theory, the time average total energy density of the three Au-coated SiNR array structures were calculated by 2D FEM. There are two important constituents: the LSP modes and the grating effects should be considered for understanding their corresponding reflectance spectra. The coupling of LSP with light can enhance or quench emission at different incident wavelengths at different locations on our structures. During the coupling processes, the incident light energies are transferred into the LSP modes. If the SP modes match with radiation modes, light emission can be efficiently enhanced. In contrast, SP dissipation leads to emission quenching. A grating structure is a good choice for controlling phase matching between LSP modes and radiation modes. The array structures we studied were fabricated by well-established silicon technology and are reproducible. Although the LSP resonance modes are sensitive to the geometries of metal/dielectric interfaces, it is still a challenge to precisely implement a particular geometry and achieve emission enhancement/quenching of a desired emission wavelength based on the LSP coupling. As exquisite design and fabrication are implemented, more efficient optical devices and newly developed circuits can be expected.

Acknowledgments

One of the authors (J W Chou) sincerely thanks Y J Lai, Guang-Yin Chen, Yan-Cheng Lin, Hui-Lin Chung, Wei-Jhih Wang, Professor Wun-Bin Jian at Department of Electrophysics, NCTU, and Yun Wan, Ruei-Fu Jao at Department of Physics, Fu Jen Catholic University, and Ching-Hsien Chen at National Nano Device Laboratories, Hsinchu, Taiwan, and Das-Kanungo Pratuysh, K Ehrhold, M Becker, S H Christiansen and U Gösele at Max Planck Institute of Microstructure Physics, Halle, Germany for experimental support and valuable discussions. This work is supported partially by the National Science Council, Taiwan, under grant no. NSC 97-2112-M009-004.

References

[1] Ritchie R H 1957 *Phys. Rev.* **106** 874–81
[2] Stern E A and Ferrell R A 1960 *Phys. Rev.* **120** 130–6
[3] Zayats A V and Smolyaninov I I 2003 *J. Opt. A: Pure Appl. Opt.* **5** S16–50
[4] Pitarke J M, Silkin V M, Chulkov E V and Echenique P M 2007 *Rep. Prog. Phys.* **70** 1–87
[5] Song J-H, Atay T, Shi S, Urabe H and Nurmikko A V 2005 *Nano Lett.* **5** 1557–61
[6] Barnes W L, Dereux A and Ebbesen T W 2003 *Nature* **424** 824–30
[7] Kneipp K, Moskovits M and Kneipp H 2006 *Surface-Enhanced Raman Scattering* (Berlin: Springer)
[8] Chuang W-H, Wang J-Y, Yang C C and Kiang Y-W 2008 *Appl. Phys. Lett.* **92** 133115
[9] Fe'lidj N, Aubard J, Le'vi G, Krenn J R, Salerno M, Schider G, Lamprecht B, Leitner A and Aussenegg F R 2002 *Phys. Rev.* B **66** 233202
[10] lbach Harald and Lüth Han 2002 *Solid-State Physics—An Introduction to Principles of Materials Science* 2nd edn (Berlin: Springer)
[11] Christiansen S H, Becker M, Fahlbusch S, Michler J, Sivakov V, Andrae G and Geiger R 2008 *Nanotechnology* **18** 035503
[12] Becker M, Sivakov V, Goesele U, Stelzner T, Andra G, Reich H J, Hoffmann S, Michler J and Christiansen S H 2008 *Small* **4** 398–404
[13] Maier S A, Kik P G, Atwater H A, Meltzer S, Harel E, Koel B E and Requicha A G 2003 *Nat. Mater.* **2** 229
[14] Bozhevolnyi S I, Smolyaninov I I and Zayats A V 1995 *Phys. Rev.* B **51** 17916
[15] Jin Jianming 2002 *The Finite Element Method in Electromagnetics* 2nd edn (New York: Wiley)
[16] Johnson P B and Christy R W 1972 *Phys. Rev.* B **6** 4370–9
[17] Wooten Frederick 1972 *Optical Properties of Solids* (New York: Academic)
[18] Christiansen S H, Chou J W, Becker M, Sivakov V, Ehrhold K, Berger A, Chou W C, Chuu D S and Gösele U 2009 *Nanotechnology* **20** 165301